Journal of Hard Tissue Biology 26[4] (2017) 311-318

CODEN-JHTBFF, ISSN 1341-7649

Original

Antibacterial Activity and Biocompability of Zinc Oxide and Graphite Particles as Endodontic Materials

Silvia Noemí Kozuszko[1,2)]*, María Alejandra Sánchez[1)]*, María Inés Gutiérrez de Ferro[3)], Ana María Sfer[4)], Ana Paula Moreno Madrid[1)], Kiyofumi Takabatake[5)], Keisuke Nakano[5)], Hitoshi Nagatsuka[5)] and Andrea Paola Rodríguez[1)]

[1)] Laboratorio de Medios e Interfases (LAMEIN), Departamento de Bioingeniería, Facultad de Ciencias Exactas y Tecnologías (FACET),Universidad Nacional de Tucumán, Consejo Nacional de Investigaciones Científicas y Técnicas, Argentina
[2)] Catedra de Anatomía y fisiología Patológicas de la Facultad de Odontología, Universidad Nacional de Tucumán, Tucumán, Argentina
[3)] Cátedra de Microbiología y Parasitología. Facultad de Odontología, Universidad Nacional de Tucumán, Tucumán, Argentina
[4)] Departamento de Estadística. Facultad de Ciencias Exactas y Tecnología Universidad Nacional de Tucumán, Tucumán, Argentina
[5)] Department of Oral Pathology and Medicine Graduate School of Medicine, Dentistry and Pharmaceutical Sciences, Okayama University, Okayama, Japan
(Accepted for publication, July 19, 2017)

Abstract: The aim of this work is to evaluate the antibacterial effect and biocompatibility of zinc oxide (ZnO) nanopaticles and graphite-type carbon (Gt) microparticles commercial powders. SEM analysis was performed to assess particles morphology. The antibacterial behavior was studied against Staphylococcus aureus (Staph. Aureus) (bacterial strain ATCC 29213) and TEM analysis of bacteria was performed to determine ultrastructural alterations; in addition, biocompatibility was evaluated in subcutaneous tissue of Wistar rats at 3, 7 and 28 d. ZnO and Gt powders exhibited antibacterial activity while TEM images of Staph. aureus showed membrane disruption followed by the release of internal content. Also, an electron-light region within the cytoplasm was observed for microorganisms treated with ZnO. Regarding biocompatibility, Gt samples induced a foreign body reaction response with presence of giant cells whereas ZnO samples showed fibroblastic connective tissue with chronic inflammatory cells and new small vessels. Also, collagen fibers and lack of capsule was observed by Trichome Masson stain. Thus, ZnO improved wound healing by enhancing tissue regeneration in contrast with calcium hydroxide control sample response which showed a fibrous tissue scar. Hence, ZnO nano-powder seems to be a potential material in the regenerative endodontic field.

Key words: Antibacterial Agents, Zinc Oxide, Graphite, Staphylococcus aureus, Foreign body reaction

Introduction

Root canal therapy is one of the most common procedures within endodontics. Here, the inflamed or infected pulp is removed and the inside of the tooth is carefully cleaned and disinfected, to subsequently be filled and sealed with different materials. Effective endodontic treatment with consequent healing depends mainly on thorough chemo-mechanical cleaning and shaping of the root canal therapy[1)]. Removal of bacteria from the root canal system is necessary for successful root canal therapy[2)]. However, it is impossible to access completely to the accessory canals and lateral ducts considering their sizes and irregularities in shape. Therefore, materials used in this stage should be capable to penetrate into all small canals, to have antimicrobial effects, to present high biocompatibility, low toxicity and to be promoters of bone formation[3)]. Due to these limitations, new sealers, irrigation solutions and intracanal dressing have been developed to improve and complement the mechanical debridement procedure. In this matter, biocompatible and antimicrobial properties turn out to be the main important features for improving endodontic treatment.

Introduction of nanosize based materials has brought new abilities into different scientific fields. In this regard, it has been documented the use of nanoparticles in disinfecting root canal space. Some studies have investigated chitosan and ZnO nanoparticles in endodontic disinfection and have obtained positive results[4,5)]. It is known, that ZnO nanoparticles have selective toxicity to bacteria but exhibit minimal effects on human cells[6)]. Moreover, it has been reported that the size and surface of carbon-based nanomaterial (nanoparticles, fullerenes, single-walled carbon nanotubes, graphene oxide) play a significant role in the antibacterial activity[7-10)]. Graphite has been evaluated as a biomedical material in heart valves, biosensors and joints[11)]. In combination with poly (vinyl alcohol) hydrogel it was also studied for fixation of artificial cornea[12)]. Hence, we believe that graphite composites could represent a suitable candidate as an endodontic biomaterial.

It is known that antibacterial activity of nanomaterials is inversely proportional to the size of the nanoparticles involved[13)]. ZnO has shown to have the same mechanism in the antibacterial activity as well as in human cell toxicity[14)]. Hence, a very small particle could have the best antibacterial effect and, at the same time, could be more related to enhanced host tissue damage. For this, particle size is crucial for endodontic applications.

Until now, several methods have been used to evaluate the biocompatibility of endodontic materials. One of the most practical and widely used methods is the implantation of the material into the subcutaneous connective tissue of rats. The local effect of the materials

* Equal contribution.
Correspondence to: Dr. Andrea Rodriguez, Laboratorio de Medios e Interfases (LAMEIN), Departamento de Bioingeniería, Facultad de Ciencias Exactas y Tecnologías (FACET), Universidad Nacional de Tucumán, Consejo Nacional de Investigaciones Científicas y Técnicas, Argentina; Tel: +543814364120; E-mail: aprodriguez@herrera.unt.edu.ar

can be evaluated by the histopathological examination of tissue response around the implant[15]. In this research, calcium hydroxide ($Ca(OH)_2$) is used as the positive control regarding its antimicrobial effect, biocompatibility, physical properties, solubility and periapical healing effect[16].

Regarding endodontic materials, there is currently no commercially available material that joins all needed properties for a successful endodontic treatment. Because of this, the main goal of this work is to evaluate the antibacterial effect and biocompatibility of ZnO and graphite-type carbon (Gt) powders. All of them were compared with the well-known response of $Ca(OH)_2$. For antibacterial assay, Gram-positive Staphylococcus aureus was selected because it is one of the most frequently isolated species in primary endodontic infections

Materials and Methods

Powder materials used in this work were the following: pure zinc oxide (ZnO, Sigma-Aldrich, Argentina), graphite (Sigma-Aldrich, Argentina) and calcium hydroxide ($Ca(OH)_2$, Farmadental, Argentina). In all cases biological evaluation was performed according to international standards. For antibacterial assay, Staph. aureus bacterial strain ATCC 29213 was used; and for biocompatibility assay, all samples were implanted in subcutaneous tissue of Wistar rats. All animal experiments were approved by Universidad Nacional de Tucumán Animal Care and Use Committee.

Scanning Electron Microscopy

The morphology of ZnO and Gt particles was characterized by scanning electron microscopy (SEM Zeiss Supra 55VP, Germany) operating at a high voltage of 15 kV. The samples were sputter coated with gold before SEM imaging. Micrographs were taken at low and high magnification to have a detailed overview of the particle morphology.

Microbiological Assay

The experimental procedure was performed in accordance with ISO-22196. Before running antibacterial sensitivity assay, fresh culture medium, agar plates, PBS, distilled water and Poly methyl-methacrylate (PMMA) discs were prepared and sterilized.

To prepare Luria-Bertani (LB) broth, 10 g/l of sodium chloride, 5 g/l of yeast extract and 10 g/l of trytone/peptone from casein were weighted and placed into a precipitation glass. Then distilled water was poured and the system was magnetically stirred up until dissolution. The broth was then autoclaved at 121ºC for 20 min and subsequently stored at 2-8ºC for no more than 1 month. To prepare LB agar plates, 14 g/l of agar-agar was weighted and added with the other ingredients to solidify the LB growth medium. Once the agar medium was dissolved and sterilized, the liquid was quickly poured onto petri dishes. Agar solidifies below 60ºC, reason why this step was performed while the agar was still warm. Subsequently petri dishes were cooled down at room temperature and then stored at 2-8ºC upside down to avoid condensed droplets to fall on the sterile gel. Phosphate buffer saline (PBS) was prepared by mixing 8 g/l of sodium chloride, 0.2 g/l of potassium chloride, 1.15 g/l of di-sodium hydrogen phosphate anhydrous and 0,2 g/l of potassium di-hydrogen phosphate anhydrous. All these salts were weighted and dissolved in distilled water.

Staph. aureus was inoculated in LB broth at 37°C for 18 h. PMMA was used to prepare 5 mm diameter disks which were used as substrates for testing each material. A measure of 1 mg of ZnO, Gt and $Ca(OH)_2$ was individually spread on top of the disks followed by a 10 µl-drop of bacteria strain with a concentration of 109 CFU/ml. Also, a bare PMMA disk and one containing amoxicillin were used as controls in this experiment. After 2 h of incubation, bacteria were recovered from each disk by immersing each sample in 1 ml of PBS in Falcon tubes and thoroughly vortexed for 1 minute. Then, 100 µl were pipetted from each tube and further dissolved in 900 µl of fresh LB broth placed in Eppendorfs tubes. After a short vortexing, 10 µl of each tube were pippeted and dropped on LB agar plates which were subsequently incubated. Colony forming units (CFU) were counted after a 18-hour incubation period at 37°C aerobically and CFU/ml were calculated, results were analyzed statistically using One way Anova followed by Tukey test.

Transmission Electron Microscopy

The collected controls and treated cells were fixed with Karnovsky fixer[17]. The samples were washed 3 times with phosphate buffer and then treated with 2% osmium tetra oxide overnight. After eliminating the remaining solution, the samples were washed 3 times with distilled water and immersed in phosphate/acetate buffer for 30 min in darkness. The remaining solution was again discarded, and the dehydration process was conducted with 70, 90 and 100 % of alcohol. The fixed cells were embedded with resin. Ultrathin sections were cut with ultra-microtome; the samples were double stained with uranyl acetate during 3 min and in citrate for 2 min[18] and further observed using a Zeiss EM 109 TEM (Zeiss, Germany).

Biocompatibility examination in vivo

In order to ensure reproducibility, the experimental procedure was performed in accordance with ISO-10993-6. Nasogastric tubes from Silmag® with the following dimensions: external diameter 1.4 mm; internal diameter 0.4 mm and length 5 mm, were used. Fifteen 2-month-old male rats Wistar weighting 200±30 g were randomly selected. All procedure was developed in accordance with the Guide for the Care and Use of Laboratory Animals 8th edition[19]. The animals were anesthetized by intra-peritoneal administration of ketamine hydrochloride (40 mg/kg) and xylazine hydrochloride (20 mg/kg). The dorsal skin was shaved and disinfected with solution of 10% iodine-povidone solution (Phoenix SAIC, BA, Argentina). Two 8 mm long incision per animal were made through the skin with a scalpel along with the vertebral axis. On each incision, two subcutaneous pockets were prepared by blunt dissection at each side of the incision. ZnO and Gt materials were mixed with physiological solution to obtain a paste which would facilitate the tube filling. Each silicon tube was filled with the corresponding powder and then sterilized. An empty tube and a tube containing $Ca(OH)_2$ were used as controls for all experiments. Each tube was carefully placed into a pocket to a depth of 20 mm from the incision to prevent smearing of the test material on the outer tube areas. After material implantation, the wounds were sutured with ETHILON™ Nylon Suture monofilament blue. All animals received normal diet and water during the entire study period.

Animals were euthanized by anesthesia overdose after 3, 7 and 28 d for tissue response examination. The implants were removed together with the surrounding tissues and immersed in 10% neutral buffered formalin (pH 7.4). After fixing for 24 h, the samples were processed for routine histological evaluation. Paraffin blocks were oriented parallel to long axis of the tubes and longitudinal serial section of approximately 5-µm thick were cut from the middle of the implant and stained with hematoxylin and eosin and Masson's trichrome stain. To evaluate the tissue response, sections of the borders of each tube were analyzed by optical microscopy. The controlled variables were inflammatory reaction, necrosis, fibrosis tissue, calcification and foreign

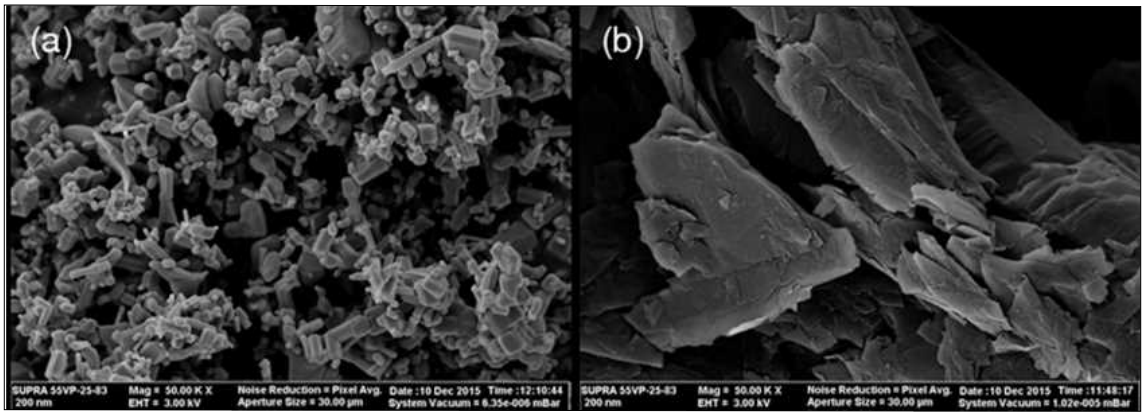

Figure 1.SEM examination of experimental material. (a) ZnO particles with cylindrical shape and 50-400 nm in size, (b) Gt particles in the form of irregular sheets and micrometric sizes.

body cell response. According to ISO 7405:1997 standard, the tissue and inflammatory reactions were graded as follows: 0= None: No inflammatory cells infiltration 1= Mild: Scattered chronic inflammatory cells without tissue changes 2= Moderate: Focal inflammatory cell infiltration with tissue changes but without necrosis 3= Severe: Severe infiltration of inflammatory cells 4= Abscess: Abscess formation[20,21].

All specimens were digitally photographed under a light microscope, and Image Pro Plus software was used as a toolkit to measure the variables necrosis. For fibrosis tissue, calcification and foreign body cell response scoring 0were: 0= absent and 1= present. The result was analyzed statistically by Kruskal-Wallis Test.

Results

Scanning Electron Microscopy

Surface topography of ZnO nanoparticles was characterized by scanning electron microscopy. The nanorods were found to be approximately 50 nm in diameter and 400 nm in height (Fig. 1a). The Gt surface topography was also analyzed showing irregular sheets particles with average sizes in the order of microns (Fig. 1b).

Microbiological Assay

Fig. 2 shows the bacteria inhibition of Staph. aureus after being in contact with bare PMMA disk, Amoxicilin, ZnO, Gt and $Ca(OH)_2$ powders. Cells count was determined as log10 CFU/ml by colonies formed on LB agar plates. In general, reduced inhibition effect was observed for all the powder tested. A 10-times reduction of CFU/ml was observed for ZnO and Gt powder after two h of incubation of bacteria in contact with powders. Significant inhibition in growth was detected between the PMMA control disk and all the other tested materials. As expected, the former bare PMMA disk showed normal bacteria proliferation while the $Ca(OH)_2$ negative control disk showed perfect inhibition of Staph. aureus growth on all experiments. Moreover, there was no significant difference ($p<0,05$) in cell number (CFU/ml) determined between ZnO and Gt powder. For this assay amoxicillin, a broad-spectrum antibiotic, was chosen as another control sample.

Transmission Electron Microscopy

TEM experiments were carried out to observe the direct membrane damage and intracellular structure change. The intracellular structure of the untreated Staph. aureus cells which were in contact with the bare PMMA disk (Fig. 3a,b). The typical round-shaped cells showed unanimous electron density. The outer membrane layer of the cell envelope and inner protoplasm were clearly visible. Also, the outer

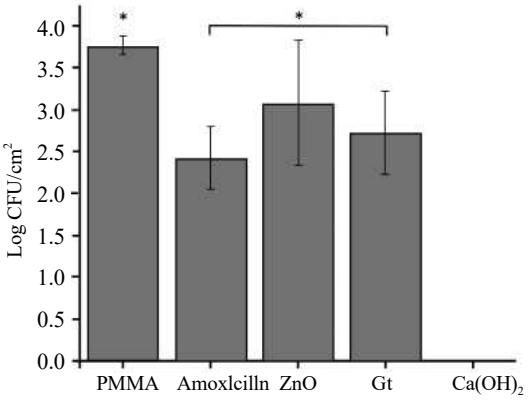

Figure 2. Effect of ZnO and Gt powder on S. aureus growth. Cells count was determined as log10 CFU/ml by colonies formed on LB agar plates. Amoxicilin, $Ca(OH)_2$ and a bare PMMA disk were used as control samples. Mean ±SD are plotted, (*) indicates significant difference in value.

membrane layer showed to be smooth and continuous. When cells were exposed to ZnO powder, significant membrane damage and intracellular structure change could be seen (Fig. 3c,d). Moreover, release of the internal cell material and difference in the internal cytoplasm density could be observed. In general, cells treated with ZnO powder showed that the outer membrane layer was neither intact not clearly visible. Also, the cytoplasm membrane shrank and detached from the cell wall slightly. This behavior was not evidence neither in the control cells or in cells treated with Gt powder. The latter showed microorganisms with both, a disruptive membrane layer with a corrugated shape (Fig. 3e,f) and normal cells without evident changes.

Histomorphological evaluation

Silicone group

At 3 d, a thin layer of necrotic tissue, scanty neutrophils new vessels, and lymphocytes were observed in direct contact with the material. At 7 d, the inflammation-free fibrous tissue was seen in direct contact with silicone. At 28 d, fibrous capsule appeared to be all over the material.

Calcium hydroxide group

At 3 d of implantation, the necrotic tissue was observed surrounding the material (Fig. 4a). Moreover, polymorphonuclear neutrophils, newly formed vessels and lymphocytes were evident as well. At 7 d, necrotic tissue, polymorphonuclear and the neutrophils were scanty (Fig. 4b).

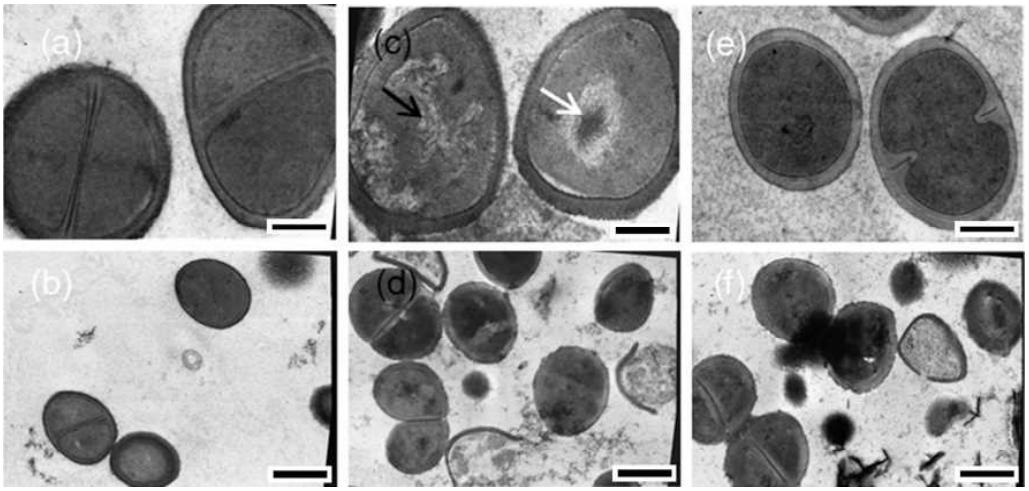

Figure 3. TEM images showing the ultrastructural effect of ZnO and Gt powders on S. aureus. Bacteria untreated in contact with PMMA disks (3a-b); in presence of ZnO powder (3c-d); and in presence of Gt powder (3e-f), at 34300X and 22800X, respectively. Ultrastructure damage is seen for ZnO and Gt samples. Microorganisms treated with ZnO showed an electron-light region with a condensed substance in the center (marked with an arrow). Scal bars=200nm

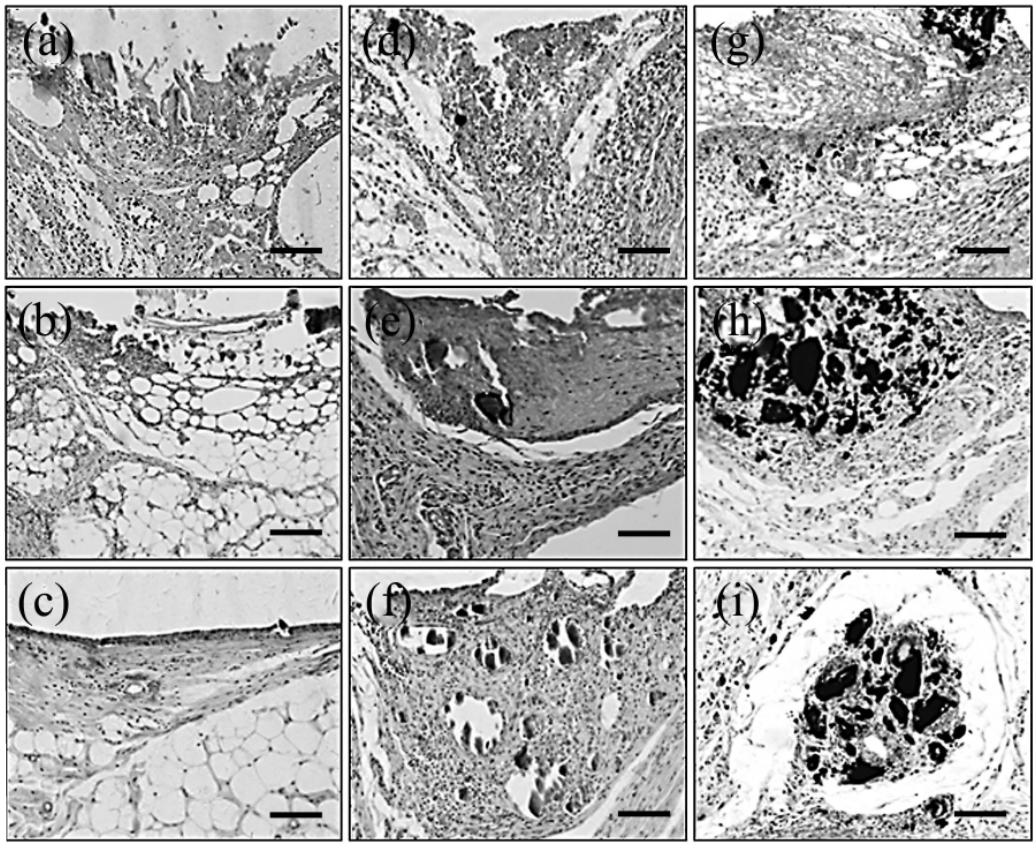

Figure 4. Histological response of $Ca(OH)_2$,ZnO and Gt samples. a) $Ca(OH)_2$ at 3(a), 7 (b) and 28 (c) ds showing an initial necrosis, inflammation response and later healing reparation by fibrotic tissue; ZnO at d 3(d) with necrosis at material contact and infiltration of inflammatory cell, ZnO at the d 7(e) presenting necrotic tissue, inflammatory cells and vessels neo-formation, ZnO a d 28 (f), showing particles surrounded by connective fibrous with angiogenesis and inflammatory cells; Gt at d 3(g), showing material displacement from the implanted tubes with scanty necrotic tissue and infiltrated neutrophils, Gt at d 7(h), particles are surrounded with chronic inflammation and macrophages giant cells, Gt at d 28(i), particles are surrounded by giants cells and a thin partial fibrous capsule (H&E). Scal bars=50μm

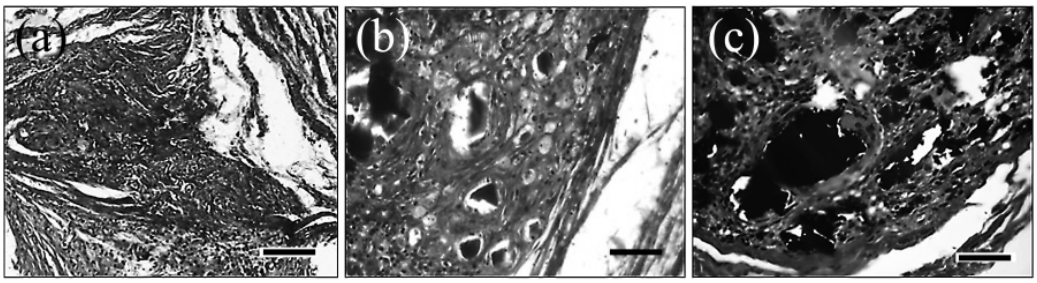

Figure 5. Presence of collagen fibers by Masson stain at 28 ds. (a) Connective fibrous showing fibrous collagenous and little vessels formation for $Ca(OH)_2$ samples, (b) presence of fibrous collagenous matrix showing the material particles, neovascular formation and inflammatory cells for ZnO samples, (c) material surrounded by giants cells and few collagen fibrous with a thin capsule for Gt samples, Masson. Scal bars=50μm

Table 1. Inflammatory scores attributed to the materials in each rat (R) at different experimental period.

	3d					7d					28d				
Groups	R1	R2	R3	R4	R5	R6	R7	R8	R9	R10	R11	R12	R13	R14	R15
Calcium Hydroxide	4	4	4	4	4	3	4	4	4	3	1	1	1	1	1
Silicone	4	4	4	4	4	1	1	1	1	2	1	1	1	1	1
Zinc Oxide	4	4	4	4	4	4	4	4	4	4	3	3	3	3	3
Graphite	4	4	4	4	4	3	4	3	4	4	3	3	3	3	3

(0) None: No inflamatory cells infiltration, (1) Mild: Scattered chronic inflammatory cells without tissue changes, (2) Moderate: Focal inflammatory cell infiltration with tissue changes but without necrosis, (3) Severe infiltration of inflammatory cells, (4) Abscess: Abscess formation

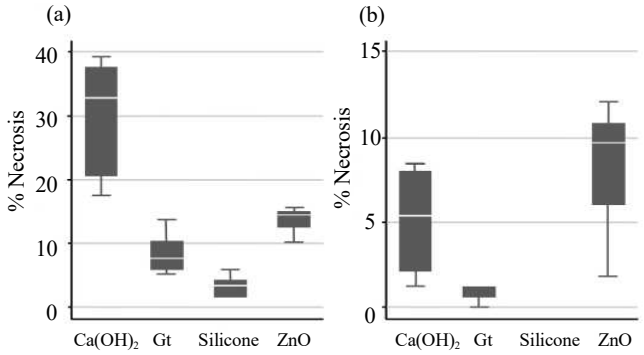

Figure 6. Necrotic tissue percentage for all samples. Statistical study of necrotic tissue at 3 ds(a) and 7 ds (b). Ca(OH)2 shows the highest percentage of necrotic response for 3 ds. At 7 ds an increased percentage was observed for ZnO nanoparticles over control sample

The granulation tissue was formed with presence of few lymphocytes. At 28 d, fibrous tissue with scanty vessels formation was presented all around the end portion of each tube. Furthermore, three of the five samples presented fibrosis and calcification (Fig. 4c). The Masson's trichrome stain allowed detecting collagen fibers within the tissue (Fig. 5a).

Zinc Oxide Group

At 3 d, the samples showed necrotic tissue around the material. Moreover, inflammatory reaction was also observed (Fig. 4d). At 7 d, enhance necrosis and inflammatory reaction was detected as well as material displacement (Fig. 4e). At 28 d, particles were detected to surround fibroblastic connective tissue together with chronic inflammatory infiltration, new small vessel formation and no fibrous capsule (Fig. 4f). Trichome Masson stain demonstrated the presence of abundant collagen fibers and no capsule shape was evidenced (Fig. 5b).

Graphite group

At 3 d, Gt samples showed material displacement and necrotic tissue. A moderate inflammatory reaction was observed. The tissue was infiltrated with neutrophils and few macrophages. The new small vessels were also observed (Fig. 4g). At 7 d, the material was also released from the implanted tubes. A chronic inflammation and the presence of macrophages containing the tested materials were revealed. Moreover, giant cells were found surrounding particles material, scanty vessels were evidence without formation of fibrous tissue (Fig. 4h). At 28 d, giant cells were seen to be in direct contact with material released from the tubes. Also, it was observed macrophages phagocyting graphite particles with a partial and thin fibrous capsule (Fig. 4i). Also, scanty collagen fibers and a marked capsule formation were observed by the Trichrome Masson stain (Fig. 5c).

The Inflammatory reactions scores attributed to the materials in each experimental period (Table 1) and the statistical analysis determined that samples were significantly different at 7 and 28 d with p=0.0027 y p=0.0003, respectively.

Histomorphometrical evaluation

At 3 d, necrotic tissue was revealed in a great percentage of the study area, being the highest percentage in $Ca(OH)_2$ samples followed by ZnO, Gt and the lowest percentage corresponded to silicone sample, being significantly different, $p<0.001$, (Fig. 6a). At 7 d, necrosis had the highest percentages in the treated parts from ZnO, followed by $Ca(OH)_2$ and then Gt, being all of them statistically different, $p = 0.0034$, (Fig. 6b). At 28 d, necrosis was absent.

Discussion

Root canal therapy represents a standard treatment that involves removing dental pulp, control considering it is the gold standard for biocompatibility and antibacterial endodontic tests[22,23] decontamining residually infected tissue through biomechanical instrumentation and root canal obturation using a filler material to replace the space that was previously composed of dental pulp. Gutta-percha is typically used as a filler material as it is malleable, inert and biocompatible. However, traditional gutta-percha has certain shortcomings including leakage, root canal reinfection, and poor mechanical properties[7]. Therefore, new fillers and composites are widely being studied to overcome these issues. As an initial evaluation of a new endodontic materials, we designed this study to assess antimicrobial performance of ZnO and Gt compared with $Ca(OH)_2$, where the latest was chosen as the positive

Various bacterial strains can be encountered during reinfection scenarios following root canal therapy. Therefore, gram-positive Staph. aureus strain was selected as the model bacterium, as it has been previously observed in endodontic failure cases[24,25]. Different antimicrobial susceptibility testing methods are known and most of them are done in aqueous media or cell culture media and the antibiotic needs to be in a liquid form[26]. When testing powders, the main problem is to have a homogeneous sample. As the addition of any surfactant substance would be controversial for the experiment, we adapted the international ISO-22196 standard to test commercial ZnO, Gt and $Ca(OH)_2$ powders against Staph. aureus. Moreover, this method shows the advantage of simulating clinical conditions where materials will be placed in aqueous medium. In this matter, the presence of powder micro-sizes agglomerations would reproduce clinical conditions.

ZnO is an environmental-friendly material which has been used in medical applications such as cancer treatments and DNA detection[27,28], and nowadays is widely being studied for dental applications[29,30]. In endodontic treatment, it is well known that particle size plays a key role on root canal disinfection. In the nano-scale, ZnO have shown bactericidal effect on numerous Gram-positive and Gram-negative bacterial strains[31,32]. Proposed mechanism for its anti-bacterial activity include the induction of H_2O_2, a strong antioxidizing agent[33,34], disruption of cell membrane and leakage of its cytoplasm contents[31] as well as internalization of nanoparticles[35]. Moreover, ZnO

nanoparticles have selective toxicity to bacteria exhibiting minimal effect on human cells[36]. It is known that ZnO is nearly insoluble in water, it agglomerates immediately in contact with water due to the high polarity, so micro-sizes aggregation can be present and hence, ZnO properties may change[26]. For this, we selected ZnO nanoparticles as the base of an endodontic material in the present work.

Graphite represents one of the main allotropic forms of carbon along with diamond. It is comprised exclusively by carbon atoms organized as infinitive layers called graphene sheets. Carbon nanomaterials such as fullerenes, carbon nanotubes or graphene, other carbon allotropic forms, have been widely studied regarding their toxicity towards bacteria and human cells[37-39]. Carbon nano-sized, were used to enhance the performances of implants, as tissue engineering scaffolds[40,41] and as composites on human dental follicle stem cells[42]. However, in general, their biological applications depend on the synthesis method and functionalization[42]. In contrast, few toxicity studies of graphite were performed. Liu and co-workers tested the antibacterial activity of graphene-based nanomaterials in aqueous dispersion towards E. coli. Here, graphene oxide showed to have more than 2.5-fold loss of bacteria viability compared with that of graphite[43]. The smaller activity of graphite could be attributed to the aggregation of graphene sheets, which for this material are in the micro-sizes leading to a sizes dependent toxicity. Additionally, when nanoparticles are tightly chemically bonded to a suitable matrix, as for example grapheme sheets within graphite, they can still demonstrate unique e.g. antibacterial properties but their environmental risks are decreased due to the limited mobility in the environmental media. Graphite is a common and widely used material with relatively low damaging effects for human health or the environment[44]. For this and considering that to the best to the authors knowledge there is little investigation about graphite toxicity, graphite was chosen as a tested material for endodontic therapy

For the antibacterial assays, amoxicillin was used as a control. Recent studies have shown that various Staph. aureus strains can express beta-lactamase, an enzyme that hydrolyzes beta-lactams[45]. Because of this beta-lactamase expression, reported minimum inhibitory concentrations (MICs) of amoxicillin against Staph. aureus have ranged from 31.250 to over 100 μg/mL[46]. In this work we used a concentration of amoxicillin that far exceeds the MIC for Staph. aureus hence the amoxicillin should exhibit an inhibitory effect against bacteria. Hence, in order to obtain results in accordance with ISO-22196, bacteria were incubated for only 2 h in contact with the testes materials. This short incubation period was chosen in this work considering that longer ones (24h) showed no colony formation on the agar plate (data not shown). Bacterial growth in contact with the tested powders was reduced approximately in 1.5 orders of magnitude compared with bacteria growth on PMMA control disks (Fig. 2). Also, it can be seen that ZnO and Gt activities are similar to amoxicillin antibacterial activity, which suggest that both tested powders behave alike (considering there is no significant difference between them, with $p>0.05$) against Staph. aureus. Both of them with the inherit advantage of not inducing bacterial resistance.

TEM images were used to further study microorganism growth. Results showed that bacteria in contact with the bare PMMA disk presented a normal growth (Fig. 3a,b). For microorganisms in contact with ZnO powder, TEM photographies revealed that the cytoplasm membrane shrank or detached from the cell wall, cell membrane was disrupted and an electron-light region appeared in the center of the cells, with condensed material positioned in the center of it (Fig. 3c,d). A similar phenomenon occurred for silver treated E. coli and Staph. aureus cells. Feng suggested that low density region formation is a mechanism of defense, by which the bacteria conglomerates its DNA to protect it from toxic compounds when the bacteria sense a disturbance of the membrane[36].

It is known that the replication on DNA molecules is effectively conducted when DNA molecules are in a relaxed state as seen in figure 3, a bacteria in contact with PMMA control samples. In a condensed form, like the one seen in microorganism treated with ZnO, DNA molecules lose their replicating activity which would explain one of its antibacterial action mechanisms. Interestingly, more research should be done to confirm if the condensed material corresponds to DNA molecules, (Fig. 3d). Hence, this behavior could be due to the formation of micro-sizes ZnO clusters due to material agglomeration. The presence of bigger particles would also have antibacterial activity. Although, evidence of cell damage and morphology changes in bacteria treated with ZnO, makes it clear that some particles were still in the nano-sizes. Hence, the reduction on CFU seen for bacteria in contact with ZnO could be due to: 1) alteration in the normal distribution of DNA molecules as a response of external toxic micro-sizes compounds leading to a reduction in proliferation rate, and 2) diminution in the amount of viable cells due to nano-sizes particles that penetrate and disrupt cell membrane producing leakage of its cytoplasm contents.

On the contrary, Gt plaques showed some membrane disruption in a few cells but no modification in the cytoplasm distribution was seen (Fig. 3e,f), which would suggest that the antibacterial mechanism could be due to a direct contact with the material and hence mechanical disruption of membrane, or due to environmental alterations which would lead its disruption. Gluthatione (GSH) is a cell antioxide widely used as an oxidative stress indicator[47-49]. Liu and co-workers used GSH oxidation to examine the possibility of ROS-independent oxidative stress mediated by graphene-based materials. They showed that the antibacterial activity of graphite is much higher than that of graphite oxide and correlated this to the electrical properties of semi-metallic graphite. The same behavior was reported in single wall carbon nanotube samples[47]. Hence, according to literature, the reduction on CFU in Gt samples performed in the current work could be due to disruption of a specific antimicrobial process by oxidizing a vital component as glutathione without ROS production, which would lead to oxidative stress and membrane disruption. Further studies should be performed in order to confirm the influence of this mechanism.

Histologically, the tissue response was assessed at 3, 7 and 28 d. Silicone tubes were used in this study considering they can be cut using a microtome and within this process keep the shape of the tissue, which constitutes an advantage over polyethylene tubes. Moreover, their biocompatibility has already been proven[50,51] and were further confirmed within this study. Calcium hydroxide was used as positive control and tissue response was the same to the Holland study[23]. In direct contact with conjunctive tissue it has shown to produce necrosis (Fig. 4a,b). Afterward, the inflammatory reaction removed the dead tissue and at 28 d, a fibrotic scar with calcification areas replaced the original architecture (Fig. 4c).

At 3 d, ZnO induced necrosis (Fig. 4d). At 7 d, the areas of dead tissue were increased (Fig. 4e and Fig. 5b), perhaps by dissolution of components of ZnO, that enhanced ROS generation and the production of pro-inflammatory cytokines (TNF, IL-6,IFNand IL-17)[52]. At 28 d, fibroblast cells, collagenous fibers and vascular proliferation were found next to the end of the tubes (Fig. 4f and Fig. 5b) which would be related to tissue regeneration, in contrast with the formation of a fibrotic scar seen in $Ca(OH)_2$ samples (Fig. 5a). Similar findings were informed by Augustine in wound skin healing model[53] and by Sousa in wound bone healing[54]. Also, the presence of inflammatory cells and new vascular formation surrounding ZnO particles (Table 1) leading to

an unresolved inflammation could be related to the dissolution of ZnO and hence ROS generation. This was also observed by Augustine[55] and Barui[56], who suggested that ROS generation, especially of H_2O_2, by ZnO nanoparticles might be the plausible mechanism for in vitro and in vivo angiogenesis. Hence, this unresolved chronic inflammation would lead to the lack of capsule.

The Gt produced initially a small area of necrosis in the connective tissue (Fig. 4i). Moreover, the necrosis was higher in those tubes implanted in contact with fatty tissue. The foreign body reaction was expressed from d 7, similar observations were reported by Anderson et al.[57], with histiocytes and giant cells that limit and engulf the material. At 28 d, the presence of giant cell reaction (Fig. 4k), infiltration of chronic cell (Table 1) and the capsule formation. The size, irregular shape, and the lack of solubility of material may be the causes of the formation of giant cells granulomas[58].

In this work, it was shown that ZnO and Gt powders have an efficient antibacterial activity. Regarding biocompatibility, Gt show the Absence of biocompatibility. On the other hand, ZnO samples demonstrated to improve wound healing by enhancing tissue regeneration. Hence, ZnO nano-powder could be considered as a potential material in regenerative endodontic field. Further studies should be carried out to verify their safety regarding long term exposures.

Acknowledgements

Financial support from National Agency for Scientific and Technological Promotion (PDTS 2016 N°574) is acknowledged. Also this study is jointly funded by the Japan Society for Promotion of Science (JSPS) KAKENHI Grant-in-Aid for Scientific Research (16K11441) and (16K20577). Further, authors would like to thank Eng. B. Felice for correcting the language of this paper and Dr. Susana Gutierrez from Dentistry Faculty for providing the Staph. aureus strain and for her advice.

Conflict of Interest

The authors have declared that no COI conflict exists.

References

1. Siqueira JF, Rôças IN, Santos SRLD, Lima KC, Magalhães F a C and de Uzeda M. Efficacy of instrumentation techniques and irrigation regimens in reducing the bacterial population within root canals. J Endod 28: 181-184, 2002
2. Yazdi KA, Sabeti M, Motahhary P, Kolahdouzan A, Shayesteh M and Shokouhinejad N. Subcutaneous tissue responses to three endodontic irrigants: A comparative study. Iran Endod J 7: 144–148, 2012
3. Saleh IM, Ruyter IE, Haapasalo M and Ørstavik D. Bacterial penetration along different root canal filling materials in the presence or absence of smear layer. Int Endod J 41: 32-40, 2008
4. Kishen A, Shi Z, Shrestha A and Neoh KG. An investigation on the antibacterial and antibiofilm efficacy of cationic nanoparticulates for root canal disinfection. J Endod 34: 1515-1520, 2008
5. Shrestha A, Zhilong S, Gee NK, and Kishen A. Nanoparticulates for antibiofilm treatment and effect of aging on its antibacterial activity. J Endod 36(6):1030–5, 2010
6. Reddy KM, Feris K, Bell J, Wingett DG, Hanley C and Punnoose A. Selective toxicity of zinc oxide nanoparticles to prokaryotic and eukaryotic systems. Appl Phys Lett 90 (21): 1–8, 2007
7. Lee DK, Kim SV, Limansubroto AN, Yen A, Soundia A, Wang CY, Shi W, Hong C, Tetradis S, Kim Y, Park NH, Kang MK and Ho D. Nanodiamond-gutta percha composite biomaterials for root canal therapy. ACS Nano 9(11):11490–11501, 2015
8. Dong L, Henderson A and Field C. Antimicrobial activity of single-walled carbon nanotubes suspended in different surfactants. J Nanotechnol 2012: 1-7, 2012
9. Shvedova AA, Pietroiusti A, Fadeel B and Kagan VE. Mechanisms of carbon nanotube-induced toxicity: Focus on oxidative stress. Toxicol Appl Pharmacol 261: 121-133, 2012
10. Gurunathan S, Han JW, Abdal Dem A, Eppakayala V and Kim JH. Oxidative stress-mediated antibacterial activity of graphene oxide and reduced graphene oxide in Pseudomonas aeruginosa. Int J Nanomed 7: 5901-5914, 2012
11. Rotern A. Effect implant material properties on the performance of a hip joint replacement. J Med Eng Technol 18 (6): 208-217, 1994
12. Liu K, Li Y, Xu F, Zuo Y, Zhang L, Wang H and Jianguo L. Graphite/poly (vinyl alcohol) hydrogel composite as porous ringy skirt for artificial cornea. Mater Sci Eng C 29: 261-266, 2009
13. Raghupathi KR, Koodali RT and Manna AC. Size-dependent bacterial growth inhibition and mechanism of antibacterial activity of zinc oxide nanoparticles. Langmuir 27: 4020-4028, 2011
14. Marjeta Č, Hribar G, Caserman S and Orel ZC. Morphological impact of zinc oxide particles on the antibacterial activity and human epithelia toxicity 52: 204-211, 2015
15. Silveira CMM, Pinto SCS, Zedebski R de AM, Santos FA and Pilatti GL. Biocompatibility of four root canal sealers: A histopathological evaluation in rat subcutaneous connective tissue. Braz Dent J 22: 21-27, 2011
16. Desai S and Chandler N. Calcium hydroxide-based root canal sealers: A review. J Endod 35: 475-480, 2009
17. Karnovsky MJ. This week's citation classic. J Cell Biol 27 (A): 137, 1965
18. Venable JH and Coggeshall R. A simplified lead citrate stain for use in electron microscopy. J Cell Biol 25: 407-408, 1965
19. Council NR. Guide for the care and use of laboratory animals: Eighth edition. The National Academies Press, Washinton,D.C, USA, 2010, pp11-88
20. Zaazou MH, Zaki DY, Mostafa AA, Mahmoud AA, Basha M and Khallaf M. In vivo biocompatibility evaluation of injectable nano-hydroxyapatite/poloxamer 407 based formulations. Part II. J Appl Sci Res 9: 5269-5276, 2013
21. Cunha SA, Rached FJA, Alfredo E, León JE and Perez DE da C. Biocompatibility of sealers used in apical surgery: A histological study in rat subcutaneous tissue. Braz Dent J 22: 299-305, 2011
22. Estrela C and Holland R. Calcium hydroxide: study based on scientific evidences. J Appl Oral Sci 11: 269-282, 2003
23. Holland R Nery M J, De Mello W and De Souza V. Root canal obturation with calcium hydroxide. Oral Surg 47: 87-92, 1979
24. Ohara-Nemoto Y, Haraga H, Kimura S and Nemoto TK. Occurrence of staphylococci in the oral cavities of healthy adults and nasal-oral trafficking of the bacteria. J Med Microbiol 57: 95-99, 2008
25. Sundqvist G, Figdor D, Persson S and Sjögren U. Microbiologic analysis of teeth with failed endodontic treatment and the outcome of conservative re-treatment. Oral Surg Oral Med Oral Pathol Oral Radiol Endod 85: 86-93, 1998
26. Sirelkhatim A, Mahmud S, Seeni A, Kaus NHM, Ann LC, Bakhori SKM, Hasan H and Mohamad D. Review on zinc oxide nanoparticles: Antibacterial activity and toxicity mechanism. Nano-Micro Lett 7: 219-242, 2015
27. Zhang Y, Nayak TR, Hong H and Cai W. Biomedical applications of zinc oxide nanomaterials. Curr Mol Med 13:1633-1645, 2013
28. Kumar N, Dorfman A and Hahm J. Ultrasensitive DNA sequence

detection using nanoscale ZnO sensor arrays. Nanotechnol 17: 2875-2881, 2006
29. Wong RH, Palamara JE, Wilson PR, Reynolds EC and Burrow MF. Effect of CPP-ACP addition on physical properties of zinc oxide non-eugenol temporary cements. Dent Mater. Acad Dent Mater 27: 329-338, 2011
30. Sevinç BA and Hanley L. Antibacterial activity of dental composites containing zinc oxide nanoparticles. J Biomed Mater 94: 22-31, 2010
31. Tam KH, Djurišić AB, Chan CMN, Xi YY, Tse CW, Leung YH, Chan WK, Leung FCC and Au DWT. Antibacterial activity of ZnO nanorods prepared by a hydrothermal method. Thin Solid Films 516: 6167-6174, 2008
32. Colon G, Ward BC and Webster TJ. Increased osteoblast and decreased Staphylococcus epidermidis functions on nanophase ZnO and TiO2. J Biomed Mater Res A 78: 595-604, 2006
33. Jones N, Ray B, Ranjit KT and Manna AC. Antibacterial activity of ZnO nanoparticle suspensions on a broad spectrum of microorganisms. FEMS Microbiol Lett 279:71-76, 2008
34. Li Q, Mahendra S, Lyon DY, Brunet L, Liga M V., Li D and Pedro JJ. Antimicrobial nanomaterials for water disinfection and microbial control: Potential applications and implications. Water Res 42: 4591-4602, 2008
35. Brayner R, Ferrari-Iliou R, Brivois N, Djediat S, Benedetti MF and Fiévet F. Toxicological impact studies based on Escherichia coli bacteria in ultrafine ZnO nanoparticles colloidal medium. Nano Lett 6: 866-870, 2006
36. Feng QL, Wu J, Chen GQ, Cui FZ, Kim TN and Kim JO. A mechanistic study of the antibacterial effect of silver ions on Escherichia coli and Staphylococcus aureus. J Biomed Mater Res 52: 662-668, 2000
37. Hurt RH, Monthioux M and Kane A. Toxicology of carbon nanomaterials: Status, trends, and perspectives on the special issue. Carbon NY 44: 1028-1033, 2006
38. Akhavan O and Ghaderi E. Toxicity of graphene and graphene oxide nanowalls against bacteria. ACS Nano 4: 5731-5736, 2010
39. Liu Y, Zhao Y, Sun B and Chen C. Understanding the toxicity of carbon nanotubes. Acc Chem Res 46: 702-713,2013
40. Nayak TR, Andersen H, Makam VS, Khaw C, Bae S, Xu X, Lai P, Ahn JH, Hong BH, Pastorin G and Ozyilmaz B. Graphene for controlled and accelerated osteogenic differentiation of human mesenchymal stem cells. ACS Nano 5 (6): 4670-4678, 2011
41. Park S, Mohanty N, Suk JW, Nagaraja A, An J, Piner RD, Cai W, Dreyer DR, Berry V and Ruoff RS. Biocompatible, robust free-standing paper composed of a TWEEN/graphene composite. Adv Mater 22: 1736-1740, 2010
42. Olteanu D, Filip A, Socaci C, Biris AR, Filip X, Coros M, Rosu MC, Pogacean F, Aib C and Baldea L. Cytotoxicity assessment of graphene-based nanomaterials on human dental follicle stem cells. Colloids Surfac B Biointerfac 136: 791-798, 2015
43. Liu S, Zeng TH, Hofmann M, Burcombe E, Wei J and Jiang R. Antibacterial activity of graphite, graphite oxide, gaphene oxide, and rduced gaphene oide. Membrane Oxidat Stress 9: 6971-6980, 2011
44. Dědková K, Janíková B, Matějová K, Čabanová K, Váňa R, Kalup A, Hundáková M and Kukutschová J. ZnO/graphite composites and its antibacterial activity at different conditions. J Photochem Photobiol B Biol 15: 256-263, 2015
45. Fuda CCS, Fisher JF and Mobashery S. β-Lactam resistance in Staphylococcus aureus: The adaptive resistance of a plastic genome. Cell Mol Life Sci 62: 2617-2633, 2005
46. Olajuyigbe OO and Afolayan AJ. Synergistic interactions of methanolic extract of Acacia mearnsii de wild. with antibiotics against bacteria of clinical relevance. Int J Mol Sci 13: 8915-8932, 2012
47. Vecitis CD, Zodrow KR, Kang S and Elimelech M. Electronic-structure-dependent bacterial cytotoxicity of single-walled carbon nanotubes. ACS Nano 4: 5471-5479, 2010
48. Lyon DY and Alvarez PJJ. Fullerene water suspension (nC) exerts antibacterial effects via ROS-independent protein oxidation fullerene water suspension (nC 60) exerts antibacterial effects via ROS-independent protein oxidation 42: 8127-8132, 2008
49. Carmel-harel O and Storz G. Roles of the glutathione- and thioredoxin-dependent reduction systems in the Escherichia coli and saccharomyces cerevisiae responses to oxidative stress. Annu Rev Microbiol 54: 439-461, 2000
50. Zmener O, Pameijer CH, Kokubu GA and Grana DR. Subcutaneous connective tissue reaction to methacrylate resin-based and zinc oxide and eugenol sealers. J Endod 36: 1574-1579, 2010
51. Osvaldo Z, Cornelis P, Kokubu G and Gabriel GD. Biocompatibilidad de conos de Resilon y conos de gutapercha en el tejido celular subcutáneo de la rata. Un estudio piloto Biocompatibility of Resilon and gutta-percha cones in the subcutaneous connective tissue of the rat. A pilot study. Rev Asoc Odontol Argent 98(5): 403-408, 2010
52. Roy R, Tripathi A, Das M and Dwivedi PD. Cytotoxicity and uptake of zinc oxide nanoparticles leading to enhanced inflammatory cytokines levels in murine macrophages: Comparison with bulk zinc oxide. J Biomed Nanotechnol 7: 110-111, 2011
53. Augustine R, Dominic EA, Reju I, Kaimal B, Kalarikkal N and Thomas S. Electrospun polycaprolactone membranes incorporated with ZnO nanoparticles as skin substitutes with enhanced fibroblast proliferation and wound healing. RSC Adv 4: 24777-24785, 2014
54. Sousa CJA, Pereira MC, Almeida RJ, Loyola AM, Silva ACA and Dantas NO. Synthesis and characterization of zinc oxide nanocrystals and histologic evaluation of their biocompatibility by means of intraosseous implants. Int Endod J 47: 416-424, 2014
55. Augustine R, Dominic EA, Reju I, Kaimal B, Kalarikkal N and Thomas S. Investigation of angiogenesis and its mechanism using zinc oxide nanoparticle-loaded electrospun tissue engineering scaffolds. RSC Adv [Internet]. Royal Soc Chem 4: 51528-51536, 2014
56. Barui AK, Veeriah V, Mukherjee S, Manna J, Patel AK, Patra S, Pal S, Murali S, Rana RK, Chatterlee S and Patra CR. Zinc oxide nanoflowers make new blood vessels. Nanoscale 4: 7861-7869, 2012
57. Anderson JM, Rodriguez A and Chang DT. Foreign body reaction to biomaterials. Semin Immunol 20: 86-100, 2008
58. Sheikh Z, Brooks PJ, Barzilay O, Fine N and Glogauer M. Macrophages, foreign body giant cells and their response to implantable biomaterials. Materials (Basel) 8: 5671-5701, 2015